Constraining the reservoir model of an injected CO_2 plume with crosswell CASSM at the Frio-II Brine Pilot

Thomas M. Daley, Jonathan B. Ajo-Franklin, Christine Doughty,
Earth Sciences Division, Lawrence Berkeley National Laboratory, Berkeley, CA

Abstract
Crosswell CASSM (continuous active-source seismic monitoring) data was acquired as part of the Frio-II brine pilot CO_2 injection experiment. To gain insight into the CO_2 plume evolution, we have integrated the 3D multiphase flow modeling code TOUGH2 with seismic simulation codes via a petrophysical model that predicts seismic velocity for a given CO_2 saturation. Results of forward seismic modeling based on the CO_2 saturation distribution produced by an initial TOUGH2 model compare poorly with the CASSM data, indicating that the initial flow model did not capture the actual CO_2 plume dynamics. Updates to the TOUGH2 model required to better match the CASSM field data indicate vertical flow near the injection well, with increased horizontal plume growth occurring at the top of the reservoir sand. The CASSM continuous delay time data are ideal for constraining the modeled spatiotemporal evolution of the CO_2 plume and allow improvement in reservoir model and estimation of CO_2 plume properties.

Keywords: CO_2, seismic, crosswell, reservoir model, petrophysics

1. Introduction

Brine aquifers provide the largest potential storage capacity for geologic sequestration of CO_2 (IPCC, 2005). In recent years, a few experiments have targeted CO_2 injection in brine formations, notably the large-scale Sleipner project (Arts et al., 2004). Large-scale projects have few, if any, monitoring wells and thus depend on reservoir models and remote monitoring (e.g. 4D seismic) to estimate the plume extent. Ideally, a sequestration monitoring program is integrated with reservoir modeling to continually improve the model and the estimates of CO_2 plume extent and residual saturation. However, at large scales, heterogeneity, resolution limits, and uncertainty can hamper monitoring efforts. Small-scale pilot injections provide an ideal opportunity to characterize reservoir processes at a scale often inaccessible in larger projects through a combination of increased resolution (both spatial and temporal) and decreased uncertainty in injection dynamics. Examples of such advantages are the Nagaoka project where crosswell tomography was utilized to estimate plume extent over about 100 meters (Saito, et al. 2006), and the Frio-I pilot where crosswell seismic tomography imaged the plume over a 30 m distance (Daley, et al, 2008). For the Frio pilot, comparing modeling results to crosswell and Vertical Seismic Profile (VSP) constrained the value chosen for field-scale residual gas saturation, an important unknown for CO_2/brine systems. A small-scale pilot can thus be used to calibrate models and techniques, at a scale intermediate between core/logs and surface seismic, for extrapolation to the larger scales.

The Frio-II brine pilot was a small scale injection of supercritical CO_2 into a high quality reservoir at the same site as the larger Frio-I test (Hovorka, et al, 2006). For the Frio-II pilot, a unique monitoring experiment was designed utilizing continuous active-source seismic monitoring (CASSM) in a crosswell configuration (Daley, et. al. 2007). A reservoir model was developed and used to predict the plume's spatial development over time. Among the important reservoir properties for CO_2 storage are residual CO_2 saturation and the associated reservoir CO_2 storage capacity. An accurate model of plume extent and spatial distribution in a small scale pilot adds confidence to model estimates of these properties. Monitoring provides constraints to improve the model accuracy, but often the only quantitative measurements available are CO_2 'breakthough' time and downhole P/T at an observation well with the addition of sparsely conducted well logs (e.g. Xue, et al 2006). CASSM data provides both high temporal sampling (nearly continuous) and sensitivity to processes happening between wells; the combination of these attributes allows CASSM to provide optimal constraints on reservoir models. For the Frio-II pilot, we show significant improvements are made to the preinjection model estimates of plume extent and spatial distribution when models are integrated and constrained by CASSM data. We present here a methodology to integrate the crosswell CASSM monitoring data with the reservoir model to obtain an improved model of the CO_2 plume (spatial extent) and the reservoir properties (CO_2 saturation distribution). The methodology uses petrophysical relationships, and notably uses patchy saturation models to link CO_2 saturation with seismic properties. We will first discuss the Frio-II pilot, then describe the TOUGH2 model and the CASSM data, then describe our integration methodology and show the constrained, updated reservoir model.

2. Frio-II Pilot Background

In September/October 2006, the Frio-II brine pilot injected about 380 tons of CO_2 into the Blue sand of the Frio formation in southeast Texas, USA. This 5 day injection was at the same site as the Frio-I pilot, but 150 m deeper. At the Frio pilot site, the fluvial Blue sand is at a depth of 1657 m, is 17 m thick, and has a dip of 18 degrees, with about 30% porosity and permeability of 1 to over 4 Darcies. The experiment site had two wells, the down-dip injector and a dedicated, up-dip, observation well, 30 m apart. The small scale of wells and CO_2 plume encouraged the use of crosswell seismic monitoring (Figure 1a). Time-lapse crosswell seismic data acquired for the Frio-I pilot showed that significant changes in P-wave velocity were caused by CO_2 displacing brine within the Frio formation (Daley, et al., 2008).

The Frio-II pilot used a unique tubing-deployed instrumentation package allowing real-time, continuous acquisition of both geochemical fluid samples (via a U-tube, Freifeld, et al, 2005) and crosswell seismic data (Daley, et al, 2007), along with downhole pressure and temperature. A detailed reservoir flow model of the Blue sand had been developed before injection for use with the TOUGH2 code (Pruess, et al, 1999). Initial preinjection modeling with TOUGH2 predicted CO_2 breakthrough time at the observation well and the spatial distribution of the plume between wells during injection. These predictions were tested by the monitoring instrumentation. The arrival time of CO_2 at the monitoring

well was measured via continuous U-tube fluid sampling with real-time gas-phase mass spectroscopy while the spatial distribution was monitored by the CASSM data acquisition (Figure 1b).

3. TOUGH2 Initial Model

For CO_2 injection into brine, multi-phase and gravity effects are significant, requiring a 3D numerical model with two-phase flow capabilities. TOUGH2 is a general-purpose numerical simulator for multi-phase, multi-component fluid and heat flow in porous and fractured media. It uses a multi-phase extension of Darcy's law that includes relative permeability and capillary-pressure effects and incorporates accurate phase-partitioning and thermophysical properties of all fluid phases and components. The Frio studies utilize a hysteretic formulation for capillary pressure and relative permeability (Doughty, 2007) and an equation of state package called ECO2 (Pruess and García, 2002), designed to treat a two-phase (liquid, gas), three-component (water, salt, CO_2) system in pressure/temperature regimes above the critical point of CO_2 (P=73.8 bars, T=31^{o}C). Although TOUGH2 has the capability to solve fully coupled fluid and heat flow problems, temperature is assumed to remain constant for the present simulations to increase computational efficiency and because field measurements showed minimal temperature change.

A detailed 3D numerical model of the multiphase, multicomponent fluid flow was developed based on a layered permeability distribution extrapolated from wireline well logs. This preinjection model used high quality logs from the recently drilled injection well. The preexisting monitoring well had limited and poorer quality open-hole well logs, along with recent cased hole logs, to provide estimates of spatial heterogeneity for the TOUGH2 model. Regional geostatistical reservoir heterogeneity estimates were also developed for the site during the Frio-I pilot. Estimates of permeability from the injection well logs were calibrated using core measurements and were found to be consistent with interference well-testing conducted prior to CO_2 injection (Figure 2). Thus the preinjection reservoir model was as good as could be obtained for any typical sequestration project with limited well data.

The model has variable lateral spatial resolution (1 m near the wells; 2 m in the region between the wells) and is oriented with one axis parallel to the line joining the injection and observation wells (Figure 3). The higher resolution near the wells decreases numerical dispersion and facilitates incorporating heterogeneous porosity and permeability distributions.

This model generated a time-series of simulated saturation distributions for five days of CO_2 injection at an average rate of 0.9 kg/s (76 T/day), which could subsequently be transformed into models of time-varying geophysical properties. Figure 3 shows the CO_2 saturation distribution calculated with the initial model for 0.4 days after beginning injection. Given this model, a petrophysical relationship between CO_2 saturation and seismic velocity is necessary to forward model the CASSM results.

4. CASSM Data

Crosswell CASSM uses fixed location source and sensors in boreholes to continuously monitor seismic waveforms as they are modified by changing reservoir conditions. At Frio-II, about 8 days of continuous monitoring of crosswell seismic response provided information on the spatial and temporal variation of the CO_2 plume as it migrated across different raypaths (Figure 4). The seismic source was the piezo-tube (Daley, et al, 2007), a tubing-deployed piezoelectric borehole source. The source location was chosen to be near the top of the reservoir sand, at 1657 m, to maximize spatial information relevant to the upper sand and to minimize the possibility of CO_2 accumulation in the near source volume. Seismic raytrace modeling was used to estimate the region of the reservoir expected to be monitored by a given source-sensor raypath. We assumed the volume sampled along each raypath was controlled by wavelength (about 2.5 m for 1 kHz signal in 2500 m/s background). The sensor locations included depths above and below the packer, which was deployed at the top of the reservoir sand and above the perforations, as shown in Figure 4. Twenty four hydrophone sensors were deployed, but electrical leakage limited the useable data to 13 sensors with variable spacing (5 above the packer and 8 below). Because of interference with a downhole pressure gauge, the seismic source was not run during the first 2 hours of injection to allow detailed pressure measurements. CO_2 injection began at approximately 7:30 pm, Central Daylight Time, on Sep 25, 2006 (Julian Day 268.8). The seismic monitoring system was operated intermittently (about 5-8 minutes of stacking at 4 pulses per second in every 15 minute interval) to produce data on approximately 15 minute intervals during the injection.

The primary information we extracted from our CASSM data is delay time (change in crosswell travel time) as a function of calendar time (Figure 5). As seen in Figure 5, the different raypaths show different delay time characteristics in both the magnitude of change and the time of change. Notable is the large delay-time change observed on the 1650 m sensor (at the top of the reservoir) and the near zero delay-time change seen on the 1630 m sensor (in the caprock, acting as a control point with no CO2 expected). This continuous delay time data is ideal for constraining the modeled spatiotemporal evolution of the CO_2 plume and thus improving a flow model's predictive capabilities. The CASSM data was also used with real-time in-field analysis to monitor flow and schedule fluid sampling with the U-tube. Changes in seismic amplitude and frequency content were observed but were not quantitatively analyzed within the current study. The overall changes in seismic waveforms are shown in Figure 6, which depicts a shot gather from the baseline period (blue traces) and from 63 hours after injection (red traces), with very low S/N traces not displayed. Significant reductions in apparent velocity and amplitude are visible.

5. Integration of TOUGH2 model and CASSM data

While the CASSM data set provides high temporal sampling of subsurface changes (about every 15 minutes), it has sparse spatial sampling and cannot be used to generate a tomographic image like typical crosswell surveys. A tomographic image of some geophysical property (e.g. seismic velocity) can only be directly compared to reservoir properties generated from a single time step or 'snapshot' of the reservoir model. With CASSM, the reservoir flow model can be evaluated for consistency between CASSM field data and forward models for each time-step. The key to this comparison is the petrophysical relationship between flow state (e.g. CO_2 and brine saturations, pressure) and geophysical state (eg. seismic velocity, density).

Figure 7 shows a schematic of our integration framework separated into three modules which have separate calculations. The integration starts with a flow modeling module which has an initial static reservoir model and outputs a complete flow state for a given time step. This flow state is the input to a rock physics module which uses a petrophysical model, along with CO_2 state properties and brine state properties, to generate geophysical properties for the given time step. These geophysical properties serve as the input to a geophysical simulation module which uses seismic modeling algorithms to calculate the CASSM data for this time step. After calculating a full CASSM data set (many time steps) the modeled CASSM data is compared to the field data and, when the match is unsatisfactory, the initial reservoir model is modified. At this point the comparison and modification is done using trial and error, guided by 'expert judgment' (i.e., a conceptual model and knowledge of the reservoir's geologic setting) to select the modifications. The problem itself could be addressed by numerical inversion, but at this point it is multi-valued and poorly constrained. An important constraint is the petrophysical model at the heart of the integration. For the problem of CO_2 displacing brine as pore-filling fluid, little work has been done on measuring petrophysical properties (i.e., the variation in seismic velocity with partial saturations at in-situ conditions), and most work is in carbonates (e.g., Wang, et al, 1998) and related to enhanced oil recovery. The choice of petrophysical model for CO_2 injection in brine is therefore a potentially important consideration which needs more study.

5.1 Petrophysical Model – Patchy Saturation

The primary objective of our petrophysical estimation is a reliable approach to map changes in CO_2 saturation to changes in observable seismic properties, a process which requires information on the properties of the rock frame, the characteristics of the fluid phases, their volumetric fractions, and finally their spatial distributions within the rock volume.

Because of recent work indicating inhomogeneous CO_2 distribution during small scale (core and field) injections (Benson et al, 2005, Daley et al, 2008, Lebedev, et al, 2009, Benson, 2008) we have chosen a patchy saturation fluid substitution theory. This theoretical model, initially proposed by White (1975), includes the corrections made by

Dutta and Seriff (1979), for the prediction and interpretation of seismic property changes due to partial CO_2 saturation. White's model assumes a homogeneous rock frame with spherical patches of dimension ***r*** saturated with a second fluid phase, in our case supercritical CO_2. White's model also assumes that the seismic wavelength is larger than the characteristic patch dimension and the results are dependent on seismic frequency.
The petrophysical model couples White's patchy fluid saturation model with NIST's CO_2 equation of state (Lemmon et al, 2005) and the brine property equations developed by Batzle and Wang (1992).

Figure 8a compares White's model (WDO), to three other poroelastic models commonly used to predict the properties of rocks partially saturated with CO_2 including Gassmann fluid substitution with either Reuss or Voigt effective fluid assumptions (Mavko et.al. 1998) and the so-called Biot-Gassmann-Hill model (BGH) (Hill, 1963). The elastic properties of the rock frame were selected from log and core information collected in the Blue Sand formation (base V_p = 2700 m/s, base V_s = 1200 m/s, porosity = 25%, permeability = 2 darcies). CO_2 and brine properties were calculated for *in situ* reservoir pressures and temperatures (P = 15 MPa, T = 55 ^oC). All curves show the change in V_p as a function of CO_2 saturation. The blue curve corresponds to the physical case where CO_2 is well-mixed with brine on the pore scale (Gassman + Reuss) while the green curve (BGH) is the quasi-static prediction for a partially saturated medium with macroscopic patches. All WDO calculations were made assuming a seismic frequency of 1100 Hz, an appropriate value based on spectral analysis of our CASSM data. Depending on the choice of ***r***, the WDO model ranges between these curves; the black lines in Figure 8 indicate the WDO predictions for CO_2 patch radii of 2.5 cm (dashed) and 15 cm (solid). In practice, we typically have no prior knowledge of ***r*** which leads to considerable uncertainty when attempting to estimate CO_2 saturation from changes in seismic velocity. For a decrease in P-wave velocity of 200 m/s (dashed cyan line), CO_2 saturations might be anywhere between 4 and 40% depending on the choice of patch size. Larger patch dimensions exhibit a quasi-linear relationship between V_p and CO_2 saturation whereas smaller patch size (pore-scale mixing) is very sensitive to low CO_2 saturations but insensitive to variations beyond 25%. Selecting the appropriate value of mixing length scale is required to quantitatively predict saturation from seismic measurements (and seismic properties from saturation). Based on the velocity changes observed in Frio-I crosswell tomography (Daley, et al, 2008) for saturations estimated as 20-30%, we have used a 2.5 cm patch size. Conceivably, this patch size value could come from either calibration experiments (on the core or log scale) or be constrained by field scale measurement of other complementary geophysical properties such as P-wave attenuation or electrical conductivity. Figure 8b shows the response of P-wave attenuation to saturation for the WDO model, with a clear dependence of the saturation-attenuation relation on patch size.

5.2 Forward modeling of CASSM data and updating the Reservoir Model

Using the petrophysical model, the initial TOUGH2 reservoir model was used to generate input geophysical properties to numerically model the CASSM results. The porosity values selected for the TOUGH2 reservoir model were converted into dry frame properties for the background model using empirical relationships calibrated to the available Frio sonic logs. The zones above and below the reservoir unit were assumed to be homogeneous with V_p values equivalent to the mean sonic log estimates (2650 m/s for the unit below and 2780 m/s for the unit above). The pressure dependence of frame properties was not included in the model due to the minimal pressure changes observed in the Frio II experiment. Our Equation of State/WDO model as described previously was used to model the effects of CO_2 saturation during the injection process.

Figure 9a depicts a single time snapshot of the change in P-wave velocity due to CO_2 injection corresponding to the beginning of Julian day 272 (day 272 of year 2006). Synthetic seismic travel-time datasets for the true CASSM geometry were calculated for all times using a non-linear eikonal solver based on the fast marching method (FMM)(Sethian and Popovici, 1999). The initial results were a poor match with no seismic response on the 1650 m sensor raypath, which showed the largest change in the field data (Figure 9b). This initial model also did not correctly estimate CO_2 breakthrough time, predicting 5 days versus the 2 days observed with U-tube sampling. The TOUGH2 model was iteratively updated, comparing field and modeled CASSM results. Aspects of the CASSM traveltime curves that were considered in the update include the timing (both relative and absolute) of responses as viewed by various source/receiver pairs, the point at which traveltime curves plateau, and the magnitude of observed traveltime changes. These parameters encode both spatial and temporal constraints of the plume evolution.

The permeability profile for the initial model (Figure 2) shows a high-permeability channel at depths from about 1663 to 1665 m in the injection well. After iterated refinement, the updated reservoir model includes (1) an extension of this high-permeability channel upward to about 1659 m depth, (2) a more precipitous decline in permeability at the upper and lower limits of the channel, and (3) a step structure for the top of the channel (that is, the permeability distribution is no longer simply layered, but also varies in the x direction mid-way between the two wells). This step structure was required to match the much later response time of the 1650 m sensor compared to the 1658, 1666, and 1680 m sensors, by enabling the injected CO_2 to not intersect the 1650 m raypath too soon. The CO_2-induced velocity change corresponding to the updated model is shown in Figure 10a. Figure 10b shows the CASSM results calculated from the eikonal solver for the updated model as compared to the observed field data. With this updated model, a significant difference was still observed for the CASSM data from the 1650 m sensor. However, the updated modeled data is fairly good at matching the calendar time at which each CASSM measurement is initially affected, but underestimates the magnitude of time delay. The predicted CASSM traveltimes for the refined model also tend to plateau at similar times to the observed curves suggesting that the main unexplained parameter is the magnitude of the induced velocity change for a given CO_2 saturation.

Significant modifications to overall plume geometry and saturation distribution were obtained by adding the CASSM information to the TOUGH2 model. Figures 11a and 11b depict the CO_2 distributions at day 272 for both the initial (a) and refined (b) permeability models. Notably, the refined CO_2 plume is thinner and longer following constrained modeling. The updated model also matches the observed CO_2 breakthrough time of 2 days, and remains consistent with pressure changes measured during the CO_2 injection period.

As mentioned previously, the modeled CASSM results were calculated using an eikonal solver and hence correspond to the minimum arrival time in the ray-theoretic sense. To explore the misfit in delay time magnitude we performed forward modeling of complete seismic waveforms generated using a high-order acoustic time-domain finite-difference (TDFD) simulation. A 1200 Hz Ricker wavelet was used to match the spectral characteristics of the piezoelectric source used in the field experiment. The results indicate that the low-velocity CO_2 plume is creating low-amplitude refractions that have an earlier arrival than the high amplitude 'direct' arrival picked in the CASSM field data. Because such refractions may not be picked in field data (due to low signal-to-noise ratio), they could disagree with the delay time calculated by the eikonal solver.

Figure 12 shows the full-waveform finite-difference travel times (hand picked 'peaks' from waveform data) compared to the field data. The FD CASSM predictions for the 1680, 1666, 1656, and 1630 m depth receivers are very similar in character to those calculated using the eikonal solver (Figure 10b). The 1650 m sensor displays a different response, primarily an earlier onset of change and a larger magnitude of change. The earlier onset is presumably due to the larger sampling volume that the finite-frequency wave-theoretic traveltime is sensitive to. The larger delay magnitude is due to a combination of wavelet broadening and picking the high-amplitude direct phase. If sufficient computing power is available, finite-difference forward modeling could replace the eikonal solver in the iterative process, otherwise the less compute intensive traveltime solver can be used for initial model iterations. However, the high magnitude and sudden change in the traveltimes picked from 1650 m sensor cannot be perfectly explained by limitations in ray theoretic traveltimes. One possibility is that changes in apparent phase in the field data led to inadvertent cycle skipping which generated the larger delay; close inspection of the field data for the 1650 m sensor was inconclusive with regards to this hypothesis.

Figure 13 depicts a direct comparison of the observed waveforms (panel A) to the modeled acoustic FD waveforms for the initial model (panel B) and the final model (panel C) for the 1650 m sensor in a temporal gather format. In this case, the modeled waveforms have been time-shifted to match the true first arrival at baseline. As can be seen, the improved model better captures the abrupt decrease in apparent arrival time but cannot match the magnitude or sudden onset of the change. In both model cases the coda structure is not replicated due to the neglect of structure outside the reservoir interval, mode conversions, and borehole effects.

6 Summary and Conclusions

Crosswell seismic data provides high spatial resolution measurements appropriate for small scale pilot injection tests. Calibration of reservoir models at small scales should allow more accurate extrapolation to larger spatial scales. The recently developed CASSM survey complements high spatial resolution with high temporal resolution measurements, thus further constraining the reservoir flow model. For the Frio-II pilot, we have applied the CASSM delay time measurements to improve a reservoir model of subsurface CO_2 flow properties by integrating crosswell CASSM data and traditional breakthrough information into updates of the initial model. Despite using good quality well log and core measurements, the initial flow model did not capture plume dynamics as observed in the field.

A petrophysical model based on patchy saturation was used to convert modeled CO_2 saturation to change in seismic velocity. Further constraints are necessary to accurately determine the CO_2/brine patch size. Remaining underestimation of delay time change suggests that a main uncertain parameter is the magnitude of the induced velocity change for a given CO_2 saturation.

The pattern of arrival of CO_2 along various seismic ray paths within the reservoir suggests strongly localized flow of CO_2 along preferential paths. The updated model captures this localized flow, providing an improved estimate of the CO_2 plume shape and increased lateral extent. Vertical flow is localized near the injection borehole with horizontal flow near the top of the sand, showing a strong buoyancy effect until reaching a permeability barrier. Such localized flow may limit residual CO_2 trapping, and reduce the rates of dissolution in brine and reaction with rock minerals. The increased lateral extent is important for reservoir usage and would not be fully captured by traditional use of breakthrough times at the monitoring well.

The CASSM survey is a new addition to the reservoir monitoring ‘toolkit’. The strength of CASSM, as used here, is the high temporal sampling allowing real time monitoring of flow processes. We anticipate an extension of CASSM as used here to include multiple sources, thus allowing continuous tomographic imaging. Such continuous imaging would be the next step in temporal and spatial monitoring of reservoir flow properties.

Acknowledgements:
This work was supported by the GEOSEQ project for the Assistant Secretary for Fossil Energy, Office of Coal and Power Systems through the National Energy Technology Laboratory, of the U.S. Department of Energy, under contract No. DE-AC02-05CH11231.

References:

Arts, R., Eiken, O., Chadwick, A., Zweigel, P. van der Meer, L., Zinszner, B., 2004, Monitoring of CO2 injected at Sleipner using time-lapse seismic data, Energy, 29, p1383-1392.

Batzle, M., and Wang, Z., 1992, Seismic properties of pore fluids, Geophysics, 57, p 1396-1408.

Benson, S., Tomutsa, L., Silin, D., Kneafsey, T. and Miljkovic, L., 2005, Core scale and pore scale studies of carbon dioxide migration in saline formations, Lawrence Berkeley National Laboratory Report, LBNL-59082, http://repositories.cdlib.org/lbnl/LBNL-59082.

Benson, S., 2008, Multi-phase flow of CO2 and brine in saline aquifers, Society of Exploration Geophysicists, Expanded Abstracts 27, p2839, DOI:10.1190/1.3063934.

Daley, T.M., R.D. Solbau, J.B. Ajo-Franklin, S.M. Benson, 2007, Continuous active-source monitoring of CO2 injection in a brine aquifer, Geophysics, v72, n5, pA57–A61, DOI:10.1190/1.2754716.

Daley, T.M., Myer, L.R., Peterson, J.E., Majer, E.L., Hoversten, G.M., 2008, Time-lapse crosswell seismic and VSP monitoring of injected CO2 in a brine aquifer, Environmental Geology, 54, 1657-1665, DOI:10.1007/s00254-007-0943-z.

Doughty, C., Freifeld, B. M. and Trautz, R. C., 2008, Site characterization for CO2 geologic storage and vice versa: the Frio brine pilot, Texas, USA as a case study, Environmental Geology, 54, p1635-1656, DOI 10.1007/s00254-007-0942-0.

Doughty, C., 2007, Modeling geologic storage of carbon dioxide: comparison of hysteretic and non-hysteretic characteristic curves, Energy Conversion and Management, 48, p1768-1781.

Dutta, N.C., and Seriff, A.J., On White's model of attenuation in rocks with partial gas saturation, 1979, Geophysics, 44, p1806-1812.

Freifeld BM, Trautz RC, Kharaka YK, Phelps TJ, Myer LR, Hovorka SD, Collins DJ (2005) The U-tube: a novel system for acquiring borehole fluid samples from a deep geologic CO2 sequestration experiment. J. Geophysical Research 110:B10203.
Hill, R., 1963, Elastic properties of reinforced solids : Some theoretical principles. J. Mech. Phys. Solids, Vol. 11, p. 357-372

Hovorka, S. D., Doughty, Christine, Benson, S. M., Freifeld, B. M., Sakurai, Shinichi, Daley, T. M., Kharaka, Y. K., Holtz, M. H., Trautz, R. C., Nance, H. S., Myer, L. R., and Knauss, K. G., 2006, Measuring permanence of CO2 storage in saline formations: the Frio experiment: Environmental Geosciences, v. 13, no. 2, p. 105–121.

IPCC, 2005: IPCC Special Report on Carbon Dioxide Capture and Storage. Prepared by Working Group III of the Intergovernmental Panel on Climate Change [Metz, B., O. Davidson, H. C. de Coninck, M. Loos, and L. A. Meyer (eds.)]. Cambridge University Press, Cambridge, United Kingdom and New York, NY, USA, 442 pp.

Pruess K, García J (2002) Multiphase flow dynamics during CO_2 disposal into saline aquifers. Environmental Geology 42:282-295

Pruess K, Oldenburg C, Moridis G (1999) TOUGH2 user's guide, version 2.0. Lawrence Berkeley National Laboratory Report, LBNL-43134.

Daley, T.M., R.D. Solbau, J.B. Ajo-Franklin, S.M. Benson, 2007a, Continuous active-source monitoring of CO_2 injection in a brine aquifer, Geophysics, v72, n5, pA57–A61, DOI:10.1190/1.2754716.

Daley, T.M., Myer, L.R., Peterson, J.E., Majer, E.L., Hoversten, G.M., 2007, Time-lapse crosswell seismic and VSP monitoring of injected CO2 in a brine aquifer, Environmental Geology, 54, 1657-1665, DOI:10.1007/s00254-007-0943-z.

Lebedev, M., Toms-Stewart, J., Clennell, B., Pervukhina, M., Shulakova, V., Patterson, Muller, T.M., L., Gurevich, B., Wenzlau, F., 2009, Direct laboratory observation of patchy saturation and its effects on ultrasonic velocities, Leading Edge, 28, 24-27.

Lemmon, E. W., McLinden, M. O., Friend, D. G., 2005, Thermophysical Properties of Fluid Systems, in: Linstrom, P. J., and Mallard, W. G. (Eds.), Chemistry Web Book, NIST Standard Reference Database Number 69,. National Institute of Standards and Technology.

Mavko, G., Mukerji, T., and Dvorkin, J., 1998, The Rock Physics Handbook : Tools for Analysis in Porous Media, Cambridge University Press.

Pruess K, Oldenburg C, Moridis G (1999) TOUGH2 user's guide, version 2.0. Lawrence Berkeley National Laboratory, Berkeley, CA, November, Rep LBNL-43134

Saito, H., Nobuoka, D., Azuma, H., Xue, Z. and Tanase, D., 2006, Time-lapse crosswell seismic tomography for monitoring injected CO2 in an onshore aquifer, Nagaoka, Japan, Exploration Geophysics, 37, p30-36.

Sethian, J.A. and Popovici, A.M., 1999, 3-D traveltime computation using the fast marching method, Geophysics, Vol. 64, no. 2, p. 516-523.

Wang, Z., M. E. Cates, and R. T. Langan, 1998, Seismic monitoring of a CO2 flood in carbonate reservoir: A rock physics study: Geophysics, 63, 1604–1617.

White, J.E., 1975, Computed seismic speeds and attenuation in rocks with partial gas saturation, Geophysics, 40, p224-232.

Xue, Z., Tanase, D. and Watanabe, J., 2006, Estimation of CO2 saturation from time-lapse CO2 well logging in an onshore aquifer, Nagaoka, Japan, Exploration Geophysics, 37, p19-29.

Figure Captions:

Figure 1: (a, left) This true-scale block diagram shows the geologic characteristics of the site (from Hovorka, et al, 2006). (b, right) Schematic of CASSM acquisition geometry shown with conceptual plume of CO_2.

Figure 2. Permeability data for the CO_2 injection well, with the injection zone shown as a black bar. An older observation-well log is also shown, with depth corrected for formation dip. Vertical blue lines are estimates from interference well tests (Courtesy of Dan Collins, Sandia Technologies).

Figure 3: Initial reservoir model (top) with zoom of central portion showing predicted CO_2 saturation at 10 hours after injection (bottom).

Figure 4: (left) CASSM schematic showing conceptual CO_2 plume along with well perforation and packer locations. (right) Example shot seismic gather for one temporal sample (stack of about 1500 shots – 5-8 minutes at 4 shots per second – and bandpass filtered).

Figure 5 : CASSM shot gather at two times, the pre-injection baseline (blue traces) and 63 hours after the initiation of injection (red traces). Equal gains are applied to both gathers to better display changes in amplitude.

Figure 6: CASSM delay time data for five sensors for 8 days of monitoring. CO_2 breakthrough time at monitoring well was obtained from U-tube fluid sampling at approximately hourly intervals.

Figure 7: Integration flow chart showing 3 modules (flow modeling, rock physics and geophysical simulation) used for numerical calculations to compare with field data.

Figure 8: Poroelastic Models including two patchy saturation models with different patch sizes. Velocity (A) and attenuation (B) of P-waves shows variation with patch size which could improve resolution of CO_2 saturation.

Figure 9: (a) Change in P-wave velocity at day 272 calculated from the initial TOUGH2 reservoir model. The CASSM source and sensor locations are indicated with symbols. (b) CASSM field data (symbols) and initial model data (solid line) for 5 sensor locations.

Figure 10: (a) Change in P-wave velocity at day 272 calculated from the final TOUGH2 reservoir model. The CASSM source and sensor locations are indicated with symbols. (b) CASSM field data (symbols) and final model data (solid line) for 5 sensor locations.

Figure 11: (a) CO_2 saturation calculated from initial TOUGH2 model, with CASSM source sensor locations shown by symbols. (b) CO_2 saturation calculated from final TOUGH2 model with CASSM constraints; CASSM source and sensors shown by symbols.

Figure 12. CASSM field data (symbols) and delay time data calculated with finite-difference wave propagation algorithm (solid lines) for the final TOUGH2 model at each of five CASSM sensor depths.

Figure 13. (A) Observed CASSM waveform data for receiver at 1650 m depth, compared to modeled waveforms from the starting model (B) and the final model (C). Modeled data are time shifted to match observed T_0 at baseline.

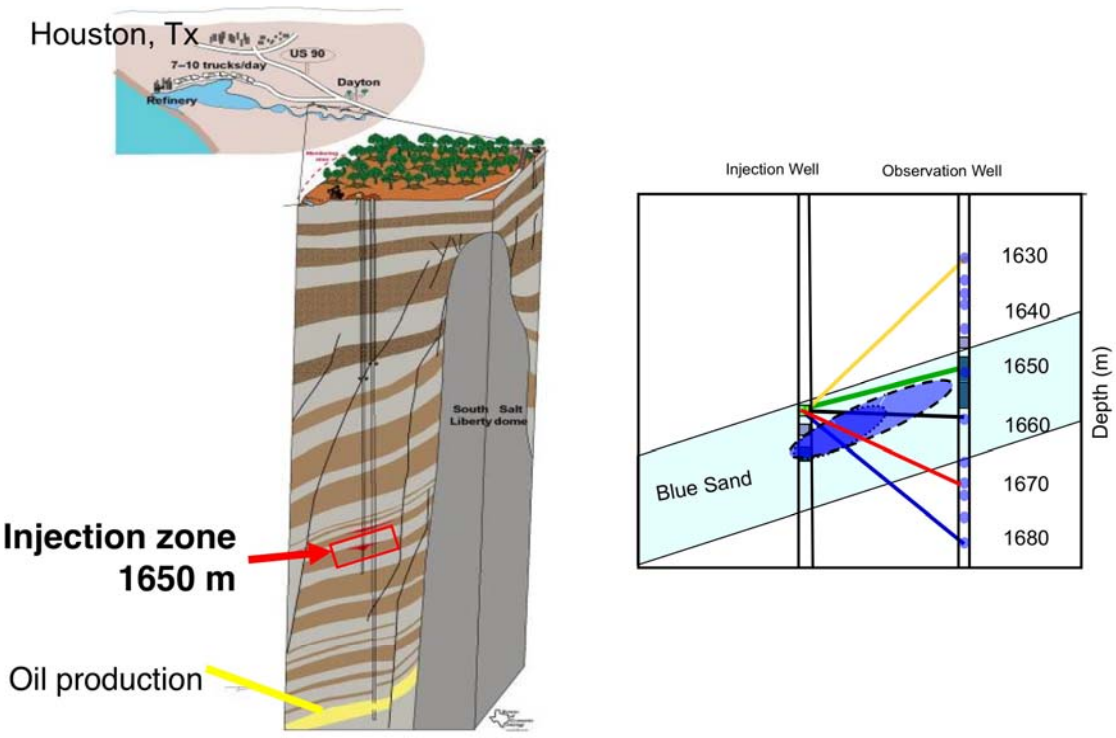

Figure 1: (a, left) This true-scale block diagram shows the geologic characteristics of the site (from Hovorka, et al, 2006). (b, right) Schematic of CASSM acquisition geometry shown with conceptual plume of CO_2.

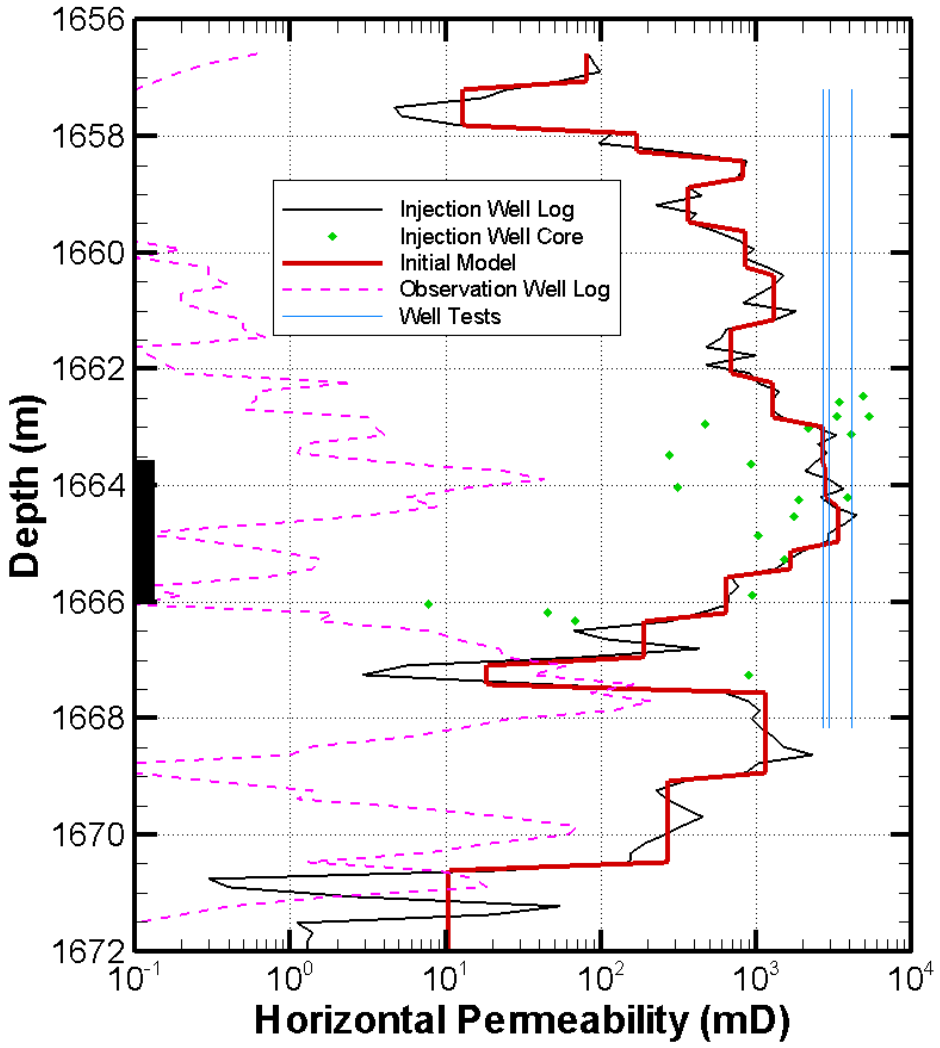

Figure 2. Permeability data for the CO_2 injection well, with the injection zone shown as a black bar. An older observation-well log is also shown, with depth corrected for formation dip. Vertical blue lines are estimates from interference well tests (Courtesy of Dan Collins, Sandia Technologies).

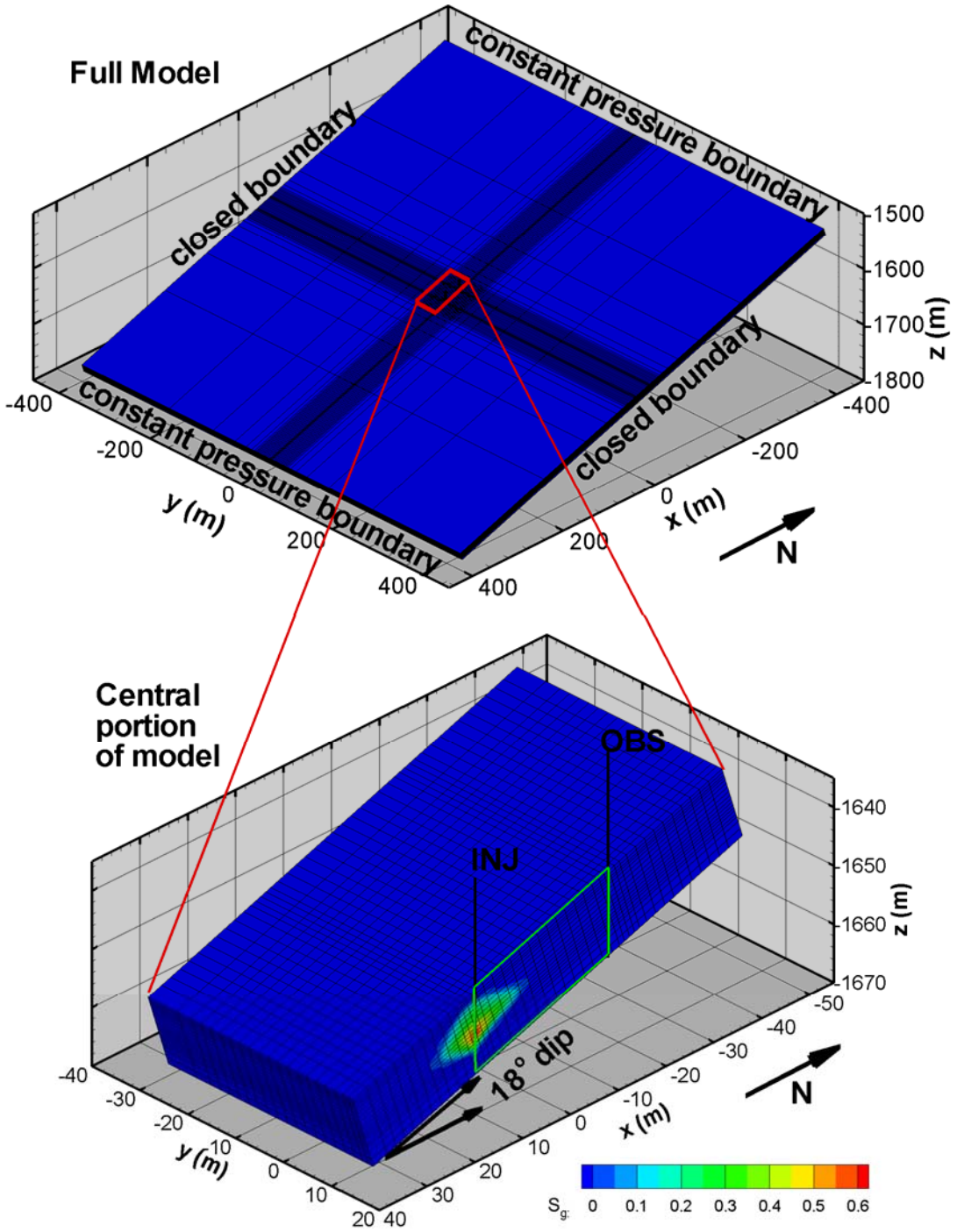

Figure 3: Initial reservoir model (top) with zoom of central portion showing predicted CO_2 saturation at 10 hours after injection (bottom).

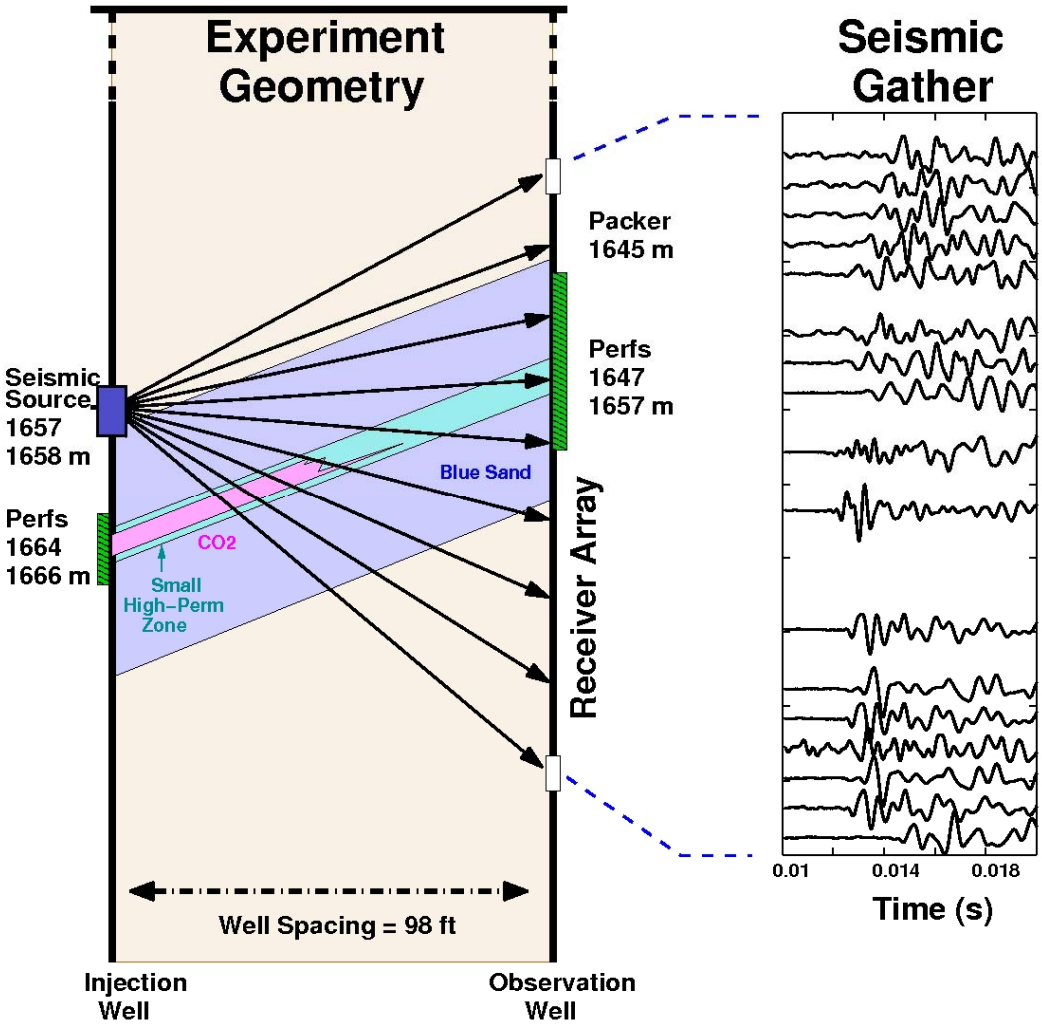

Figure 4: (left) CASSM schematic showing conceptual CO2 plume along with well perforation and packer locations. (right) Example seismic shot gather for one temporal sample (stack of 1500 shots acquired over 6 minutes) after bandpass filtering.

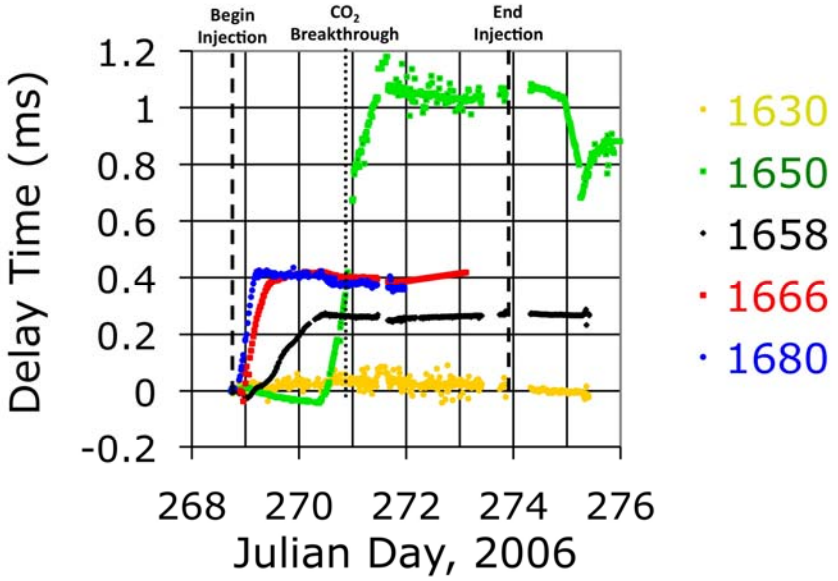

Figure 5: CASSM delay time data for five sensors for 8 days of monitoring. CO_2 breakthrough time at monitoring well was obtained from U-tube fluid sampling at approximately hourly intervals.

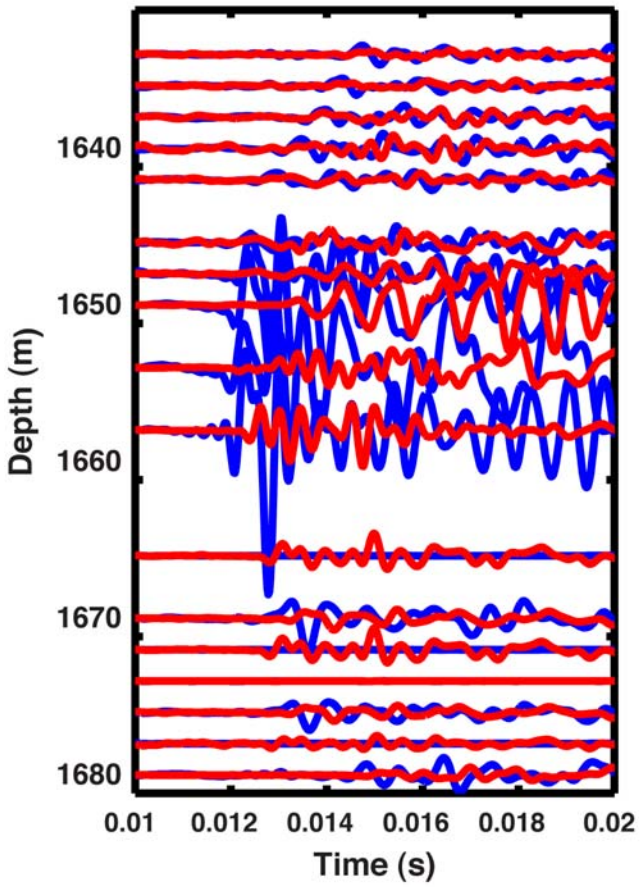

Figure 6 : CASSM shot gather at two times, the pre-injection baseline (blue traces) and 63 hours after the initiation of injection (red traces). Equal gains are applied to both gathers to better display changes in amplitude.

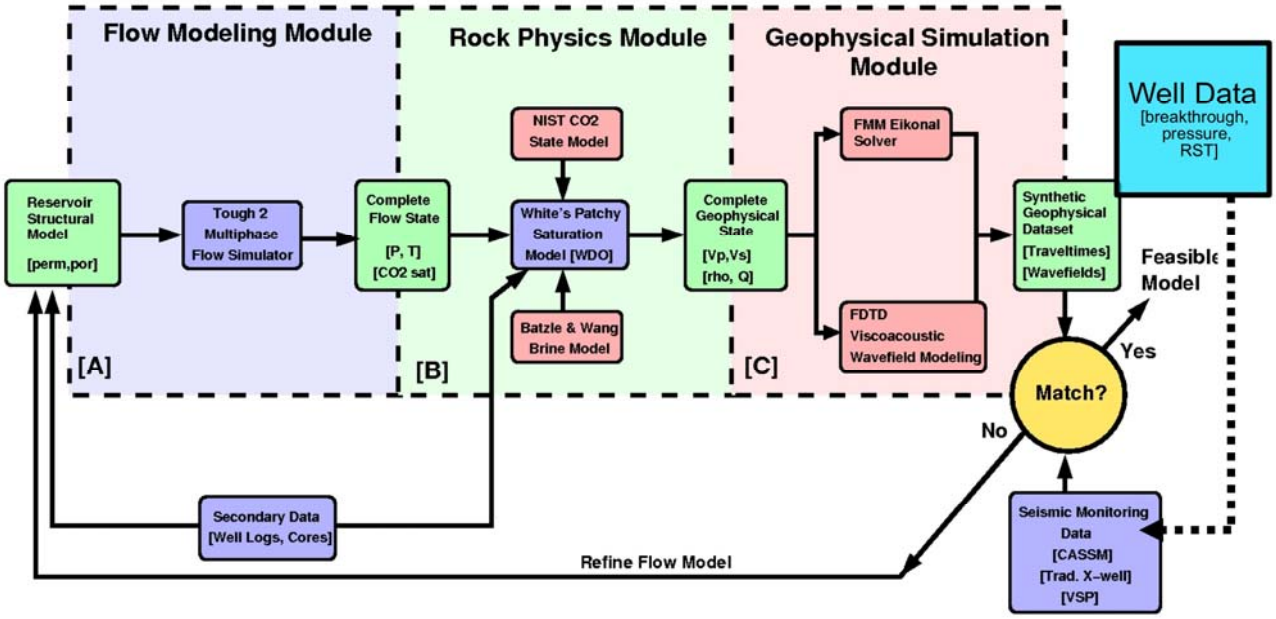

Figure 7: Integration flow chart showing 3 modules (flow modeling, rock physics and geophysical simulation) used for numerical calculations to compare with field data.

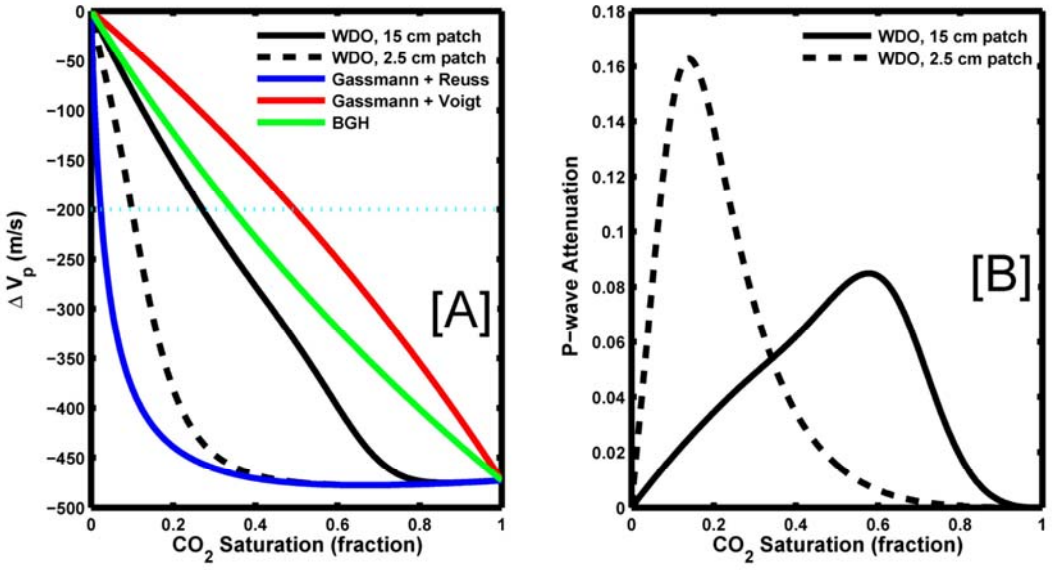

Figure 8: Poroelastic Models including two patchy saturation models with different patch sizes. Velocity (A) and attenuation (B) of P-waves shows variation with patch size which could improve resolution of CO_2 saturation.

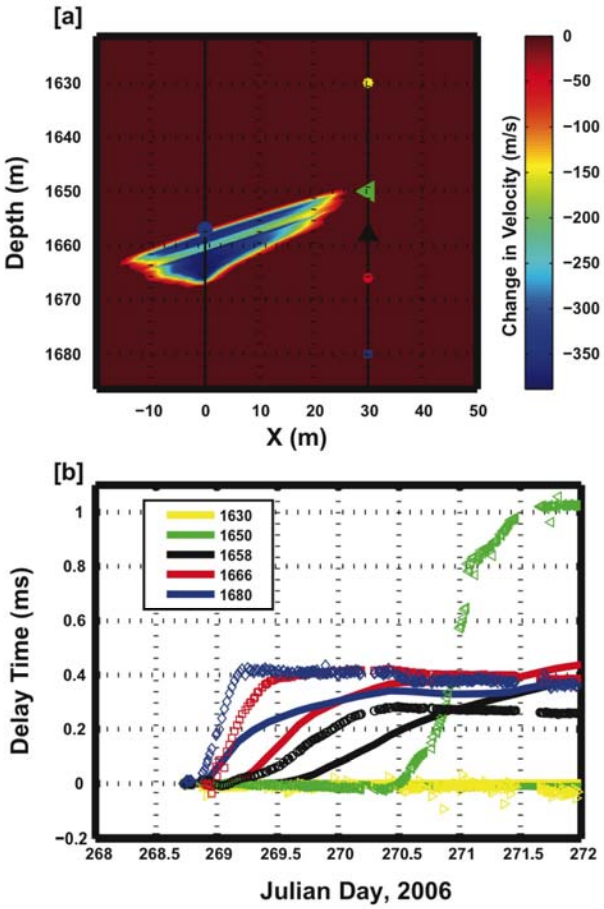

Figure 9: (a) Change in P-wave velocity at day 272 calculated from the initial TOUGH2 reservoir model. The CASSM source and sensor locations are indicated with symbols. (b) CASSM field data (symbols) and initial model data (solid line) for 5 sensor locations.

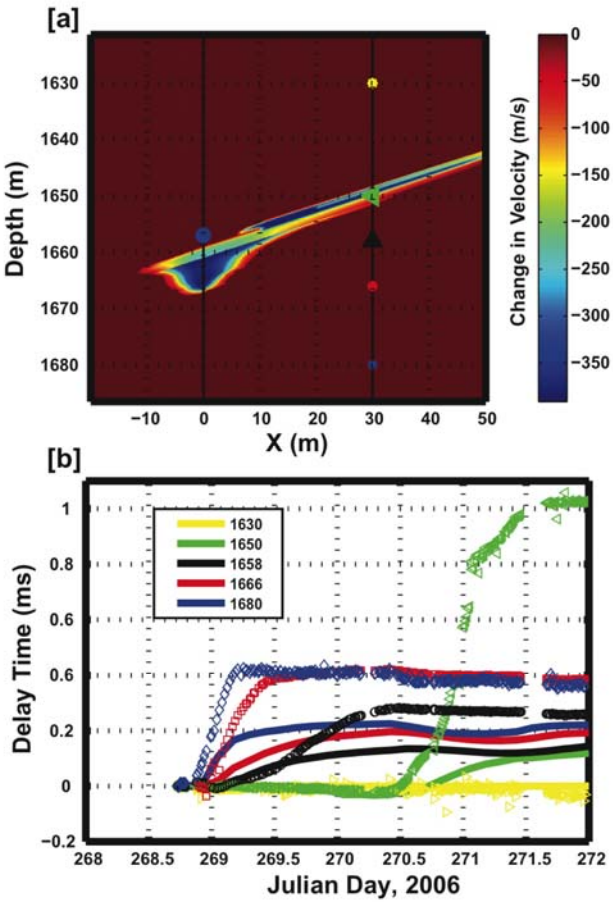

Figure 10: (a) Change in P-wave velocity at day 272 calculated from the final TOUGH2 reservoir model. The CASSM source and sensor locations are indicated with symbols. (b) CASSM field data (symbols) and final model data (solid line) for 5 sensor locations.

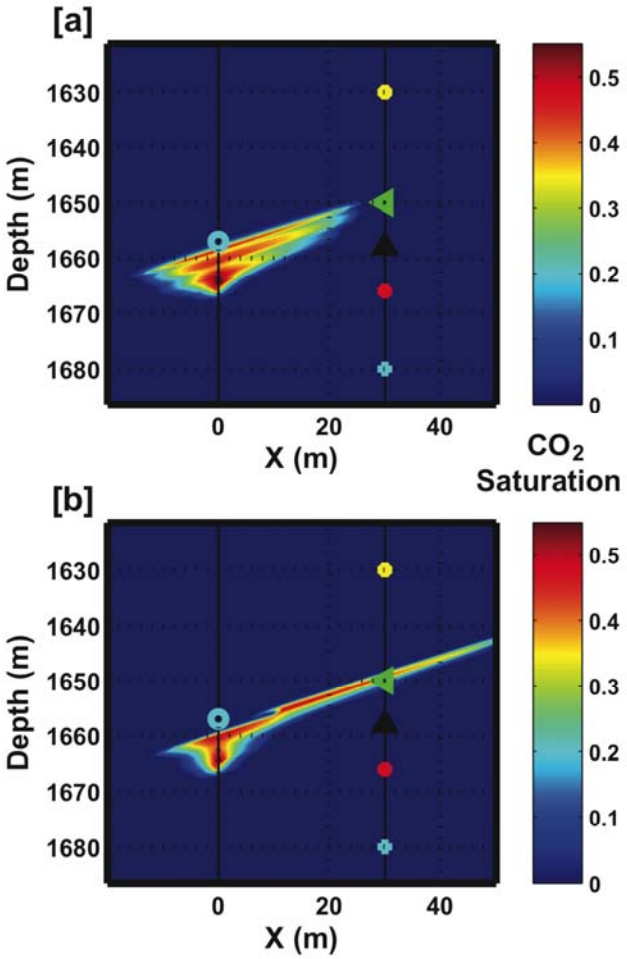

Figure 11: (a) CO_2 saturation calculated from initial TOUGH2 model, with CASSM source sensor locations shown by symbols. (b) CO_2 saturation calculated from final TOUGH2 model with CASSM constraints; CASSM source and sensors shown by symbols.

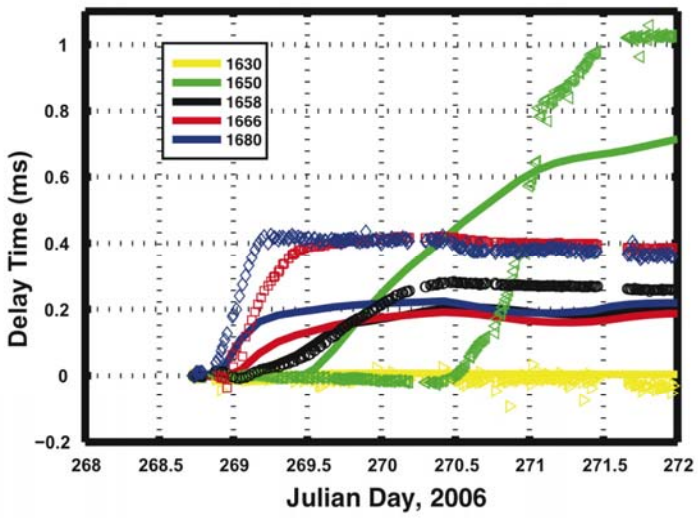

Figure 12. CASSM field data (symbols) and delay time data calculated with finite-difference wave propagation algorithm (solid lines) for the final TOUGH2 model at each of five CASSM sensor depths.

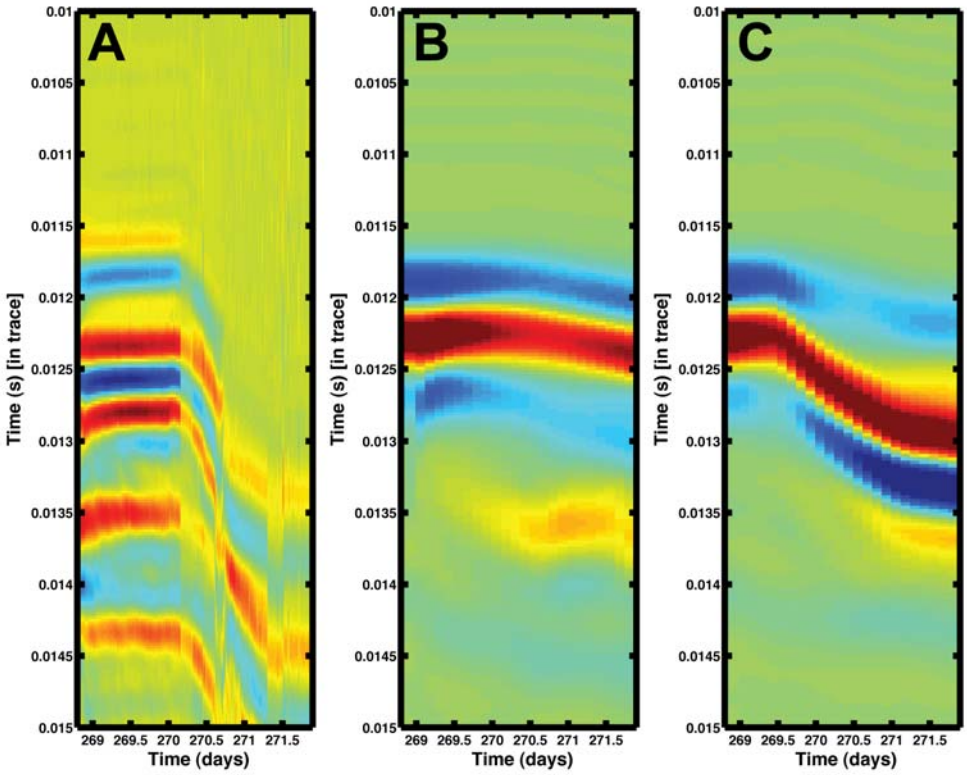

Figure 13. (A) Observed CASSM waveform data for receiver at 1650 m depth, compared to modeled waveforms from the starting model (B) and the final model (C). Modeled data are time shifted to match observed T_0 at baseline.